Title No. 121-S25

Effect of Bond Condition on Cyclic Behavior of Post-Tensioned Concrete Beams with Carbon Fiber-Reinforced Polymer Tendons

by Fei Peng, Weichen Xue, and Shulu Zhang

The lack of ductility is the main concern in the use of carbon fiber-reinforced polymer (CFRP) reinforcement as prestressing tendon in concrete members. To address this concern, a partially bonded concept has been proposed. In this approach, CFRP tendons are intentionally debonded from the concrete in the middle region of the prestressed concrete beam, while remaining bonded at each end. In this study, eight post-tensioned beams, including five beams with CFRP tendons and three beams with steel tendons, are tested under cyclic loading. Three bond conditions, including fully bonded, partially bonded, and fully unbonded, are considered. The results indicate that increasing the unbonded length of the tendon changed the failure mode from CFRP rupture to concrete crushing. There is a trend that the flexural capacity decreased with the increase of the unbonded length. The displacement ductility (μ) of partially bonded CFRP prestressed beams ranged from 5.38 to 5.70, which is significantly higher than that of the fully bonded beam (μ = 2.83) and slightly lower than that of the fully unbonded beam (μ = 6.10). Finally, by introducing a relative bond length coefficient into the ultimate tensile stress equation for internally unbonded tendons, a modified design approach for estimating flexural capacities of the partially bonded beams is proposed. The experimental flexural capacities are in close agreement with the values predicted using the modified design approach.

Keywords: carbon fiber-reinforced polymer (CFRP); cyclic behavior; ductility; partially bonded; prestressed concrete beam.

INTRODUCTION

Corrosion-induced deterioration of steel strands is one of the major reasons that the structural integrity of prestressed concrete structures is compromised before the structures reach their expected lifespan (Grace et al. 2013). Substituting steel strands with fiber-reinforced polymer (FRP), particularly carbon FRP (CFRP), offers a viable solution due to its exceptional properties such as corrosion resistance, high strength-to-weight ratio, fatigue resistance, and low relaxation (Grace et al. 2013; Peng and Xue 2018a). However, the inherent brittleness of FRP limits the ductility of structural members.

Enhancing the ductile behavior of the structural concrete members reinforced with FRP reinforcements has remained the focus of research in recent years. Various concepts have been investigated to achieve this objective, including promoting ductile compression failure through the use of fiber-reinforced concrete (FRC) (Fischer and Li 2003; Peng et al. 2023) and employing hybrid reinforcing schemes (Safan 2013; Peng and Xue 2018b). It is generally recommended to design the flexural reinforcement ratio to exceed

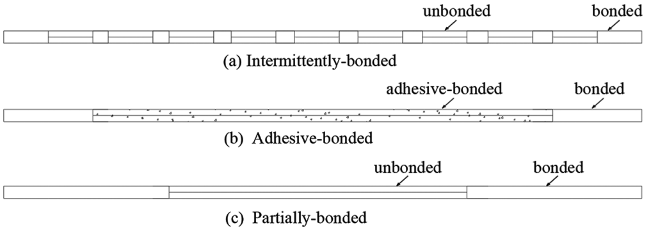

Fig. 1—Types of partial bonding of FRP tendons.

the balanced ratio (Peng and Xue 2019a; Poudel et al. 2022; Peng et al. 2023), at which the rupture of FRP tendons and concrete crushing occur simultaneously. However, employing a high FRP reinforcement ratio can be uneconomical. An alternative approach to prevent tendon rupture and improve beam ductility is the use of unbonded FRP tendons. Unbonded tendons are allowed to slip, relieving strains from critical sections and distributing them along the beam length, thereby delaying or preventing FRP tendon rupture (Grace and Abdel-Sayed 1998; Heo et al. 2013; Sun et al. 2022; Au and Du 2008). This implies that even if a prestressed concrete beam with unbonded FRP tendons has a significantly lower flexural reinforcement ratio compared to the balanced reinforcement ratio in the bonded case, concrete crushing may occur prior to FRP tendon rupture (Au and Du 2008; Lee et al. 2017). Nevertheless, the anchorage of fully unbonded FRP prestressed concrete members remains a critical challenge. Despite efforts made over the past two decades, efficient and competitive prestressing anchor systems for FRP tendons are still limited (Jeong et al. 2019).

To address these issues, the concept of partially bonded FRP systems was introduced. Lees and Burgoyne (1999) first proposed partial bonding as a means to improve the ductility of concrete beams prestressed with FRP tendons. In their proposal, partial bonding was achieved in two ways, either by intermittently bonding sections of tendons, or by coating the tendon with a resin, as shown in Fig. 1(a) and (b), respectively. The flexural behavior of fully bonded, fully unbonded, and partially bonded pretensioned concrete beams was compared by Lees and Burgoyne (1999). The study concluded that partially bonded beams exhibited an ultimate

ACI Structural Journal, V. 121, No. 2, March 2024.
MS No. S-2023-065.R1, doi: 10.14359/51740251, received July, 17, 2023, and reviewed under Institute publication policies. Pertinent discussion including author's closure, if any, will be published ten months from this journal's date if the discussion is received within four months of the paper's print publication.

load capacity equivalent to fully bonded beams and a rotation capacity comparable to fully unbonded beams. However, the construction complexity associated with these partial bonding patterns may limit their practical application. Latterly, several researchers (Rizkalla 2000; Dorian 2002) proposed an alternative partial bonding pattern, wherein the tendons were debonded from the concrete in the middle region of the beam and bonded to the concrete at each end, as shown in Fig. 1(c). This partial bonding pattern has been introduced to strengthen existing structural members using FRP strips (Choi et al. 2011a; Sharaky et al. 2015; Chen et al. 2021).

Several studies have investigated the mechanical behavior of partially bonded CFRP prestressed concrete beams. Rizkalla (2000) and Dorian (2002) conducted flexural tests on pretensioned concrete beams containing a hybrid arrangement of partially bonded CFRP tendon and nonprestressed stainless steel bars under static loading. The results indicated that an increase in the unbonded length led to a decrease in ultimate capacity while promoting improved deformability. Jeong et al. (2019) evaluated the fatigue performance of post-tensioned concrete beams with partially bonded CFRP tendons. It was found that the partially bonded CFRP prestressed beams exhibited satisfactory fatigue performance, with no signs of cracks or stiffness degradation during fatigue loading. Furthermore, the ductility index of the partially bonded CFRP prestressed beams was comparable to that of beams prestressed with steel tendons.

In summary, the partially bonded FRP reinforcing scheme offers a competitive technique in terms of ductility, end-anchored ability, and cost-effectiveness. Furthermore, the addition of fibers in concrete can further enhance the ductility of FRP prestressed concrete beams. However, there is limited research conducted on the mechanical behavior of partially bonded CFRP prestressed concrete beams. This paper, therefore, presents a detailed experimental study on FRC beams with partially bonded CFRP tendons. Eight post-tensioned beams are tested under low reversed cyclic loading. The test results are presented in terms of failure modes, hysteresis curves, skeleton curves, load capacity, displacement ductility, and energy dissipation capacity.

RESEARCH SIGNIFICANCE

Despite the competitiveness of the partial bonding concept in terms of ductility and end-anchoring ability, there is a lack of comprehensive research on the cyclic behavior of partially bonded CFRP prestressed concrete beams. The main objective of this research is to investigate the cyclic behavior the polypropylene FRC beams with partially bonded CFRP tendons. In addition, a design approach will be proposed for predicting the flexural capacity of these beams. The findings from this study will contribute to a better understanding of the cyclic performance of partially bonded CFRP prestressed concrete beams and provide a practical design tool for their structural application.

EXPERIMENTAL PROGRAM

Test specimens

In engineering practice, few concrete beams are prestressed exclusively with CFRP reinforcements due to their lack of ductility and control of crack distribution. To enhance ductile behavior and provide crack control, an alternative approach is to incorporate nonprestressed bars such as galvanized, epoxy-coated, or stainless steel (Peng and Xue 2018b). This study adopts a partially prestressed scheme where CFRP strands serve as prestressing tendons, and epoxy-coated steel bars are used as nonprestressed bars.

A total of eight post-tensioned concrete beam specimens, including five beams prestressed with CFRP strands and three beams prestressed with steel strands, were designed, constructed, and tested. Among the CFRP prestressed beams, one was fully bonded, one was fully unbonded, and the remaining beams were partially bonded. The fully bonded beam was designed to fail due to CFRP rupture, while the partially bonded beam, with the central portion of the tendon debonded from the concrete, was expected to fail through concrete crushing. All specimens were doubly reinforced, with the top flexural reinforcements chosen to produce negative flexural strength similar to positive loading cases. Each beam had a rectangular cross section of 150 x 250 mm (5.9 x 9.9 in.) and a span of 3500 mm (13.8 in.). Details of the tested beams are provided in Table 1 and Fig. 2. The test parameters included the unbonded length of prestressing tendon and the type of tendon used. In this study, all specimens were designed with a consistent partial prestressing ratio (PPR) of 0.55, which is defined as

$$\mathrm{PPR} = \frac{A_p f_{pu}}{A_p f_{pu} + A_s f_y} \tag{1}$$

where A_s is the area of steel bars in tension; A_p is the area of prestressing tendons; f_y is the yield strength of steel bar in tension; and f_{pu} is the ultimate tensile strength of prestressing tendon.

It should be noted that the effective cross-sectional area of CFRP strands differs from that of steel strands, making it challenging to maintain the same reinforcement ratio in beams with different prestressing tendon types. To investigate the influence of prestressing tendon type, the CFRP prestressed beams were designed to have the same PPR and jacking stress as the steel prestressed beams. To ensure a flexural failure mode, all specimens within the shear span were equipped with 8 mm (0.3 in.) diameter steel stirrups spaced at intervals of 100 mm (3.9 in.).

The specimens are referred to using acronyms that indicate their various characteristics. The first part of the acronym indicates the bond condition ("FB" for fully bonded, "PB" for partially bonded, and "UB" for unbonded). The second part of the acronym represents the type of prestressed tendon ("S" for steel strand and "C" for CFCC). The last part of the acronym indicates the unbonded length of the tendon, which can be 0, 1100, 1900, 2700, or 3500 mm (43.3, 74.8, 106.3, or 137.8 in.). Following this notation, Specimen PB-C-11 is a beam prestressed with partially bonded CFCC tendons, with an unbonded length of 1100 mm (43.3 in.).

Material properties

All specimens were designed with concrete with a target compressive strength of 50 MPa (7.3 ksi). The concrete used

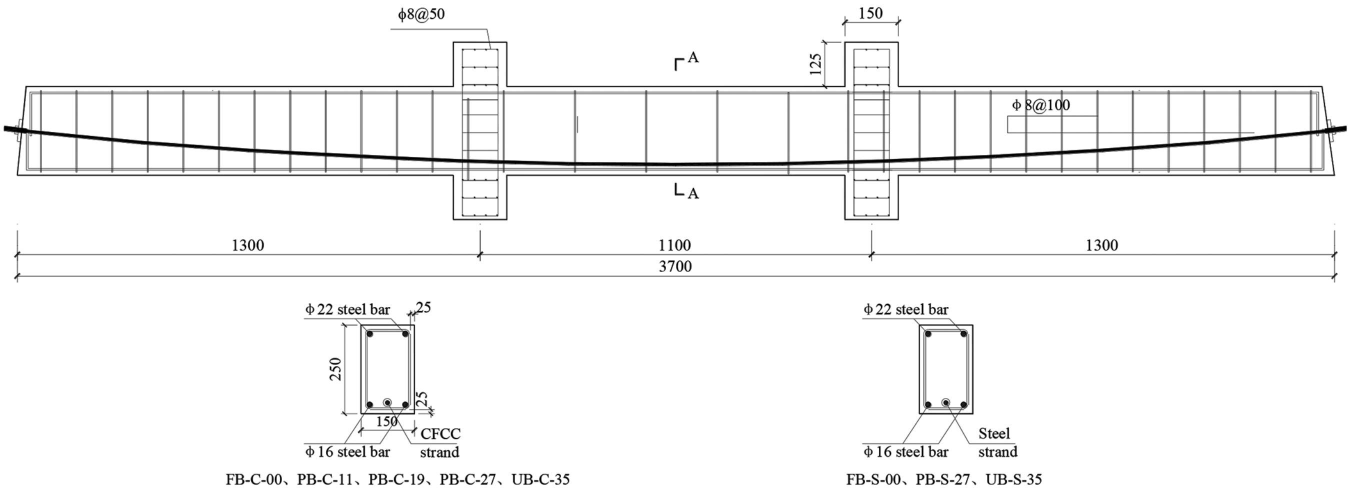

Fig. 2—Dimensions and reinforcement details of test specimens. (Note: Units in mm; 1 mm = 0.0394 in.)

Table 1—Details of specimens

Specimens	Unbonded length, mm	Tendons	Effective prestress, MPa	Top longitudinal reinforcements	Bottom longitudinal reinforcements
FB-C-00	0	$1\phi^{cfrp}12.5$	829	2F22	2F16
PB-C-11	1100	$1\phi^{cfrp}12.5$	927	2F22	2F16
PB-C-19	1900	$1\phi^{cfrp}12.5$	914	2F22	2F16
PB-C-27	2700	$1\phi^{cfrp}12.5$	894	2F22	2F16
UB-C-35	3500	$1\phi^{cfrp}12.5$	890	2F22	2F16
FB-S-00	0	$1\phi^{s}12.7$	838	2F22	2F16
PB-S-27	2700	$1\phi^{s}12.7$	880	2F22	2F16
UB-S-35	3500	$1\phi^{s}12.7$	880	2F22	2F16

Note: 1 MPa = 0.145 ksi.

Table 2—Material properties of concrete

Specimens	Modulus of elasticity E_c, MPa	Cube compressive strength f_{cu}, MPa	Splitting strength f_{st}, MPa
FB-C-00	3.62×10^4	65.20	4.62
PB-C-11	3.54×10^4	65.88	4.36
PB-C-19	3.68×10^4	61.75	4.64
PB-C-27	3.61×10^4	55.48	4.17
UB-C-35	3.79×10^4	57.76	4.64
FB-S-00	3.53×10^4	57.80	4.45
PB-S-27	3.48×10^4	58.83	4.17
UB-S-35	4.12×10^4	60.23	4.64

Note: 1 MPa = 0.145 ksi.

in this study was a FRC previously developed by the authors previously (Xue et al. 2011). The mixture design consisted of 260 kg/m^3 (16.22 lb/yd^3) of cement, 260 kg/m^3 (16.22 lb/yd^3) of grinded blast-furnace slags, 188 kg/m^3 (11.74 lb/yd^3) of water, 684 kg/m^3 (42.70 lb/yd^3) of middle grit, 1024 kg/m^3 (63.93 lb/yd^3) of gravels, and 1.8 kg/m^3 (0.11 lb/yd^3) of polypropylene fibers. The inclusion of ground blast-furnace slags in concrete with a fineness of 5×10^3 cm^2/g attempted to enhance the activity of admixtures. Additionally, the addition of polypropylene fibers (15 mm [0.6 in.] in length) with 2.3% volume fraction of cement attempted to increase the anti-dry-shrinkage cracking property of cement mortar in the hardening stage. On the day of testing, the concrete compressive strength, splitting strength, and modulus of elasticity for each beam were determined in accordance with the Chinese standard GB/T 50081 (2019). Table 2 lists the measured mechanical properties of the concrete for each beam.

The 12.5 mm (0.5 in.) diameter, seven-wire CFCC strand and 12.7 mm (0.5 in.) diameter, seven-wire steel strand were used as the prestressing tendons. The CFCC strand possessed an effective cross-sectional area of 75.6 mm^2 (0.117 in.^{2}) and a guaranteed ultimate tensile strength of 1860 MPa (270 ksi). The tensile properties of CFCC strands were determined as per ASTM D7205 (2021) with a measured tensile strength of 2400 MPa (348 ksi). The steel strand had an effective cross-sectional area of 98.7 mm^2 (0.153 in.^{2}) and an ultimate tensile strength of 1860 MPa (270 ksi). Mild steel bars were used as nonprestressed reinforcements and stirrups. Table 3 lists the mechanical properties of the steel reinforcements used in this study.

Fabrication and prestressing

A partially bonded reinforcing scheme has a portion of the reinforcement intentionally unbonded. In this study, the unbonded length of the prestressing tendon was situated within the middle portion of the simply supported beam,

Table 3—Mechanical properties of steel bars and prestressing tendons

Bar type	Designation	Yield strength, MPa	Ultimate tensile strength, MPa	Modulus of elasticity, MPa	Elongation ratio
Steel bar	Φ8	313	425	200	27.7%
	Φ16	385	550	200	29.1%
	Φ22	371	556	200	30.4%
Steel strand	ϕ^{s} 12.7	—	1861	195	5.5%
CFCC strand	ϕ^{cfrp} 12.5	—	2400	150	1.6%

Note: 1 MPa = 0.145 ksi.

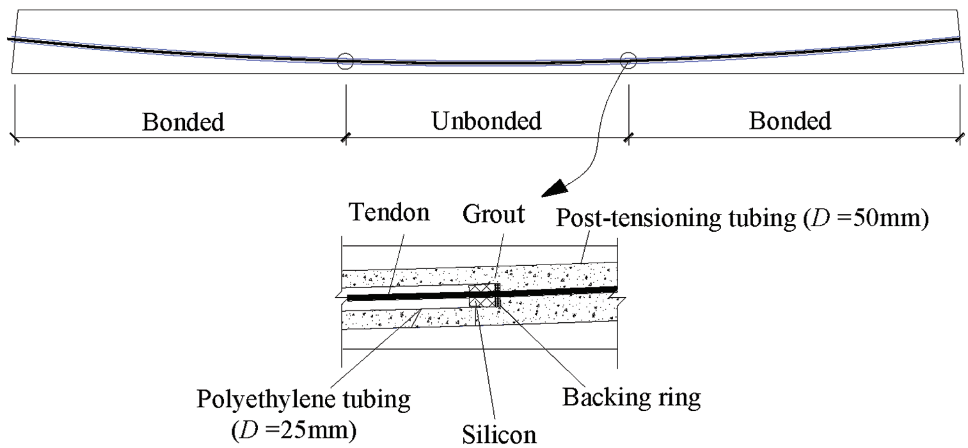

Fig. 3—Preparation of partially bonded tendon. (Note: 1 mm = 0.039 in.)

while the end portions were bonded, as shown in Fig. 3. Special preparation of the partially bonded tendons was necessary. A 25 mm (1 in.) diameter polyethylene duct was threaded over the tendon to achieve the desired unbonded length. Silicon was used to seal both ends of the duct, and electrical tape was wrapped around the silicon at both ends of the tendon to prevent concrete penetration into the duct.

The post-tensioning for CFRP was achieved using a bonded anchorage system and a hydraulic jack. The maximum permissible stress in CFRP at jacking specified in ACI 440.4R (2004) is 65% of its specified tensile strength. In this study, jacking stress of $0.55f_{pk}$, where f_{pk} represents the manufacturer provided guaranteed CFRP tensile strength, was selected. The compressive concrete strength on the day of prestressing was at least 80% of its target compressive strength. The CFRP strand was post-tensioned at one end of the beams to a target prestressing force. After prestressing, post-tensioning plastic ducts were filled with grout. On the day of testing, the effective prestress for each specimen was measured, as listed in Table 1. It was observed that the prestress losses for CFRP tendons ranged from 10 to 19%.

Test setup and instrumentation

As shown in Fig. 4, all beams were tested under four-point loading which was cyclically applied by using a hydraulic testing machine. The loading protocol, which consists of two phases in conformance with Chinese standard GB/T 50152 (2012), is presented in Fig. 5. The first phase is a load-controlled cycle, where the specimens are loaded downwardly and upwardly, respectively, until cracks formed. The second phase is a displacement-controlled cycle at a rate of 1 mm/min, in which three cycles are repeated at each step. In this phase, the specimens are loaded to multiples of Δ_y, where Δ_y is the displacement corresponding to the yielding of the tensile steel bars at bottom of the beams. During testing, the applied loads were monitored through load cells. Three linear variable differential transformers (LVDTs) with an accuracy of 0.001 mm were mounted along the beams to measure vertical deflection at the support and midspan. Electrical resistance strain gauges were mounted on the longitudinal steel bars and prestressing tendons to measure their strains.

TEST RESULTS AND DISCUSSIONS

Cracking behavior and failure modes

During the testing process, flexural cracks were initiated in the pure bending region of the tested beams. Table 4 lists the flexural cracking load for each beam. As the applied load increased, the existing flexural cracks extended in length and width along with occurrence of a few new flexural cracks. During upward loading, the cracks at the bottom closed and flexural cracks were observed at the top of the concrete at the pure bending sections. Following the yielding of mild steel reinforcements, flexure-shear cracks could be observed, and the flexural cracks continued to propagate. Subsequently, the length and width of the existing cracks continued to increase, with no new cracks forming. Eventually, a large number of vertical cracks and a few horizontal cracks could be observed around midspan sections of beams. Typical ultimate deformation of the tested beams is depicted in Fig. 6.

As expected, all beams exhibited flexural failure. With the exception of the fully bonded beam (FB-C-00), the final failure of all specimens was caused by crushing and spalling of concrete at pure bending sections, accompanied by

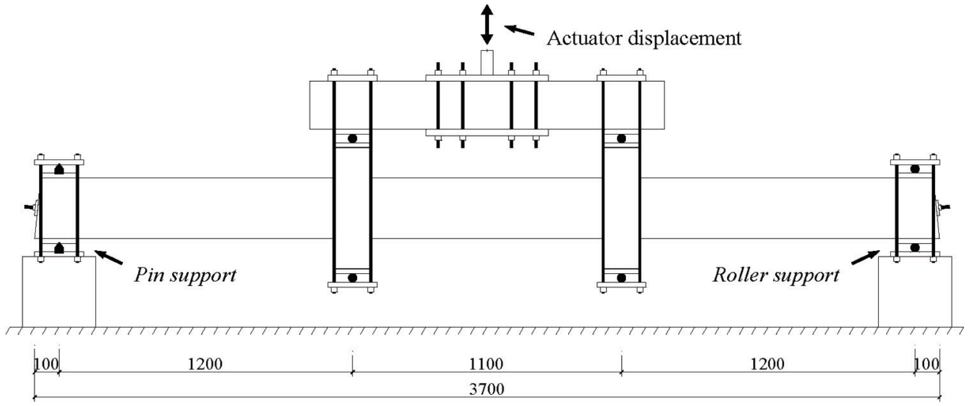

(a) Scheme proposal

(b) Final test setup

Fig. 4—Test setup. (Note: Units in mm; 1 mm = 0.0394 in.)

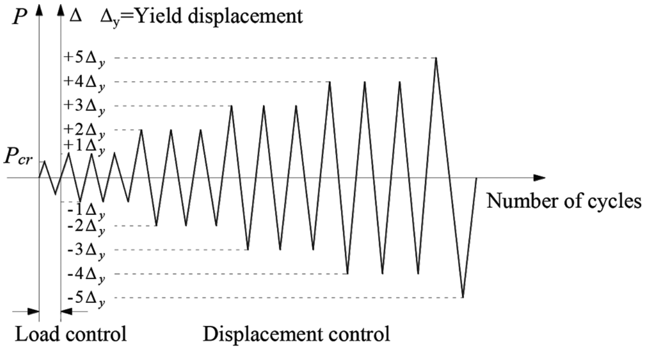

Fig. 5—Loading protocol.

buckling of longitudinal steel bars, referred to as a compression failure. The failure of Specimen FB-C-00, on the other hand, was controlled by rupture of the CFRP tendon accompanied by insignificant crushing of concrete, referred to as a tension failure. This is because the unbonded portion is free to slip, resulting in more or less equalized strain along the unbonded length of the tendon and reduced strain at the critical section. These two types of failure modes are depicted in Fig. 7. At the onset of failure, the strain of CFRP tendon in FB-C-00 was observed to approach its ultimate tensile strain. For partially bonded and fully unbonded beams, however, the maximum strain in the CFRP tendons did not exceed their ultimate tensile strain, ranging between 0.011 and 0.013.

Hysteresis curves

The load-midspan displacement hysteresis curves of all the tested beams are shown in Fig. 8. Prior to concrete cracking, the hysteresis curves were basically linear, with relatively small areas of hysteretic loops. No obvious degradation in flexural stiffness could be observed and the residual deformation was negligible. After flexural cracking of the specimens, the load-midspan displacement hysteresis curve became nonlinear. The areas of hysteretic loops became larger, indicating that energy dissipation increased. When the midspan displacement was below $3\Delta_y$, the maximum load obtained in the next two cycles was nearly the same as that in the first cycle at the same level of displacement. This indicates that the strength degradation of the beams under reverse cyclic loading was negligible. When the midspan displacement exceeded $3\Delta_y$, however, a strength reduction was observed, which can be attributed to cumulative damage resulting from the load repetition. For instance, at a displacement level of $4\Delta_y$, a strength reduction of 5.2 and 14.3% was observed in Specimens PB-C-11 and PB-C-19 under downward loading, respectively.

As observed in Fig. 8, all hysteresis curves exhibited noticeable pinching, which can be attributed to the influence of prestressing. It was found that the beams prestressed with steel strands underwent more loading cycles than those prestressed with CFRP strands. This is expected because the CFRP is an elastic and brittle material that does not exhibit yielding behavior. With the exception of the fully bonded CFRP prestressed concrete beam (Specimen

Table 4—Test results

Specimens	Loading direction	P_{cr}, kN	P_y, kN	P_{max}, kN	Δ_{cr}, mm	Δ_y, mm	Δ_u, mm	Δ_u/Δ_y	$P_{max,exp}/P_{max,pre}$
FB-C-00	↓	25.3	82.7	93.7	2.70	23.70	65.95	2.83	—
	↑	–20.0	–86.8	–100.8	–2.45	–23.35	–60.57	—	—
PB-C-11	↓	25.5	70.3	101.8	3.06	20.31	115.81	5.70	1.09
	↑	–15.0	–88.9	–93.4	–1.01	–21.82	–95.47	—	—
PB-C-19	↓	30.0	79.6	98.8	3.47	21.76	117.1	5.38	1.07
	↑	–10.5	–87.9	–88.6	–0.21	–22.99	–55.62	—	—
PB-C-27	↓	26.5	64.0	87.2	2.42	21.79	119.50	5.48	0.97
	↑	–20.0	–93.5	–94.5	–1.44	–21.82	–71.50	—	—
UB-C-35	↓	25.0	66.6	87.3	2.85	20.66	126.3	6.10	0.95
	↑	–18.0	–85.4	–86.4	–1.85	–23.54	–76.75	—	—
FB-S-00	↓	23.0	82.9	110.9	3.12	23.80	133.67	5.62	—
	↑	–18.0	–87.0	–99.1	–1.98	–21.16	–134.16	—	—
PB-S-27	↓	29.8	62.5	86.0	1.71	20.19	133.08	6.59	0.93
	↑	–23.0	–96.6	–101.0	–1.64	–21.14	–74.30	—	—
UB-S-35	↓	25.0	61.0	93.3	–3.59	19.29	135.24	7.01	0.98
	↑	–20.0	–90.3	–94.3	–1.91	–21.73	–75.92	—	—

Note: 1 mm = 0.0394 in.; 1 kN = 0.2248 kip; 1 MPa = 0.145 ksi.

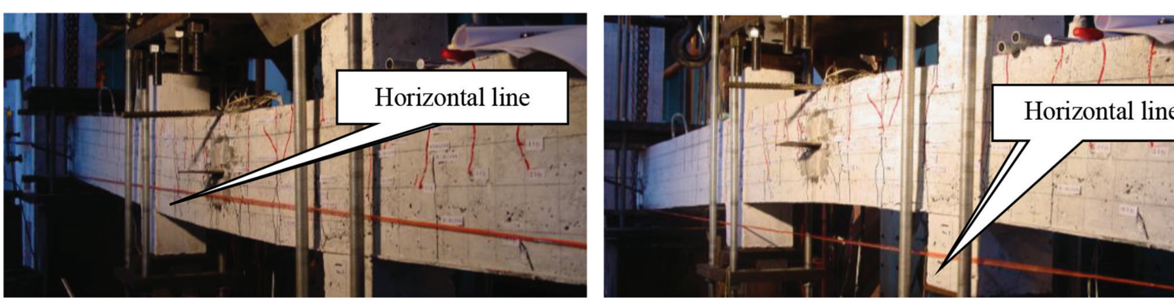

(a) downward ultimate deformation (b) upward ultimate deformation

Fig. 6—Ultimate deformation of typical test beams.

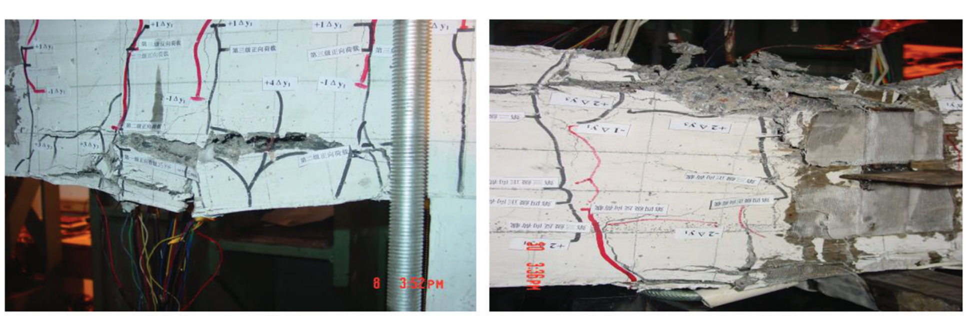

(a) tension failure (b) compression failure

Fig. 7—Typical failure modes of test beams.

FB-C-00), which failed after only three load cycles, all the CFRP prestressed concrete beams sustained no fewer than five loading cycles. This is because the fully bonded CFRP prestressed concrete beam exhibited a premature failure due to rupture of CFRP before concrete crushing.

Skeleton curves

Skeleton curves are envelopes of hysteresis curves. Generally, the skeleton curves of structural members under cyclic loading are close to those under monotonic loading in both shape and values. Figure 9 shows the skeleton curves for each specimen. Prior to cracking, the skeleton curves are approximately linear and the effects of bond are negligible because of insignificant change in tendon stress in this elastic stage.

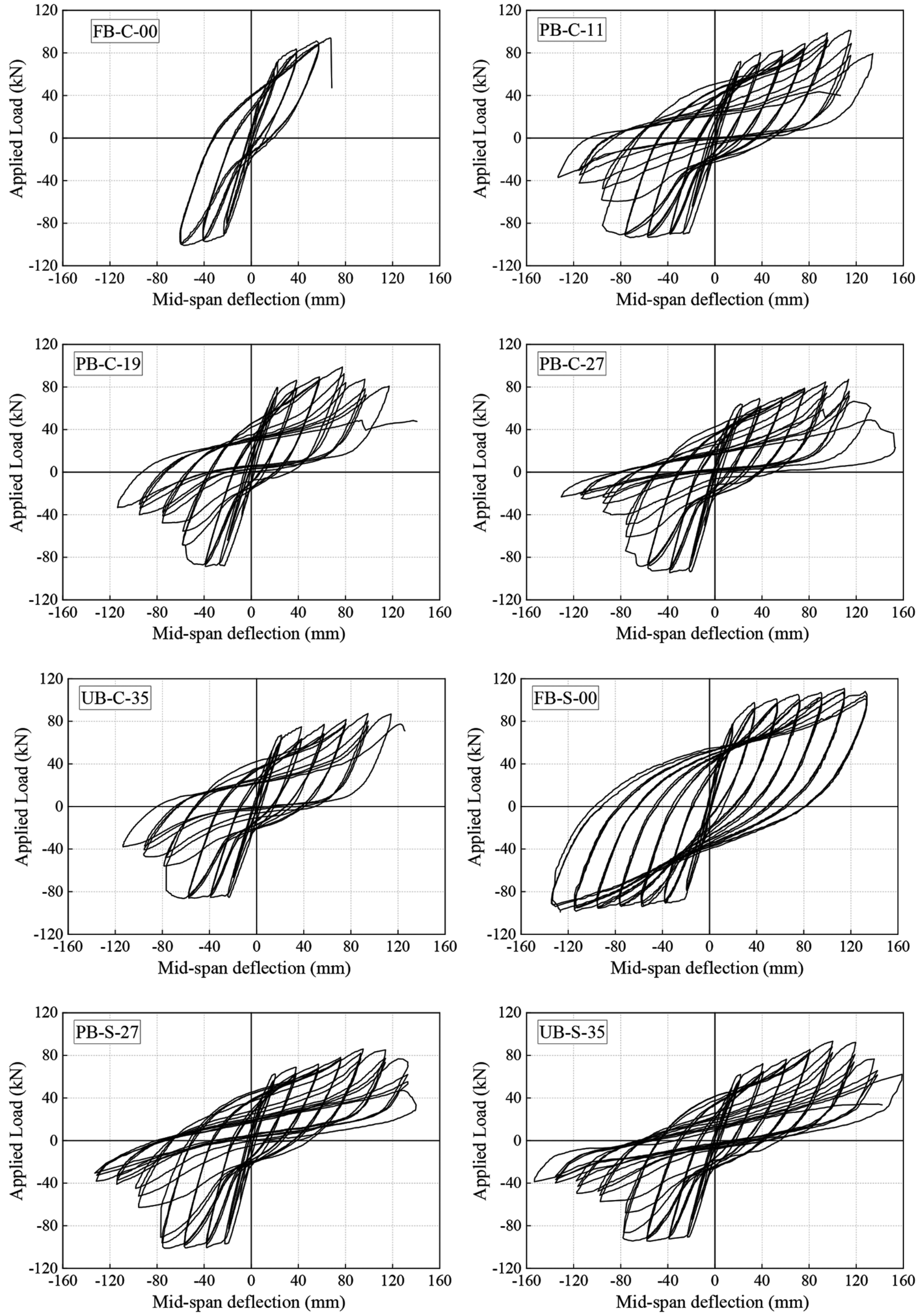

Fig. 8—Load versus deflection relationship of test beams. (Note: 1 kN = 0.2248 kip; 1 mm = 0.0394 in.)

After cracking, the loading increment lagged behind the deformation increment and stiffness degraded apparently. In the post-cracking stage, the fully bonded CFRP prestressed beams are shown to be stiffer than unbonded and partially bonded ones. This is because tendon stress increases faster in fully bonded prestressed beams than in partially bonded and unbonded prestressed beams. After yielding of the tensile steel bar, obvious inflection points could be observed in the skeleton curves. Thereafter, stiffness continued to degrade until the maximum load point. When the midspan displacement exceeded $4\Delta_y$, obvious overall strength degradation could be observed in the partially bonded and fully unbonded beams under downward loading, which was significantly different from the downward behavior. This is attributed to the fact that the prestressing tendon is placed at the bottom of the beams.

Load-carrying capacity

Table 4 lists the cracking loads, yielding loads (corresponding to the yielding of the nonprestressed steel bars), and maximum loads of the specimens. It was observed that the cracking loads under downward loading were influenced little by the unbonded length of CFRP tendons. However, a trend was observed where the maximum loads (P_{max}) decreased as the unbonded length of the CFRP tendons increased. Specifically, as the unbonded length increased

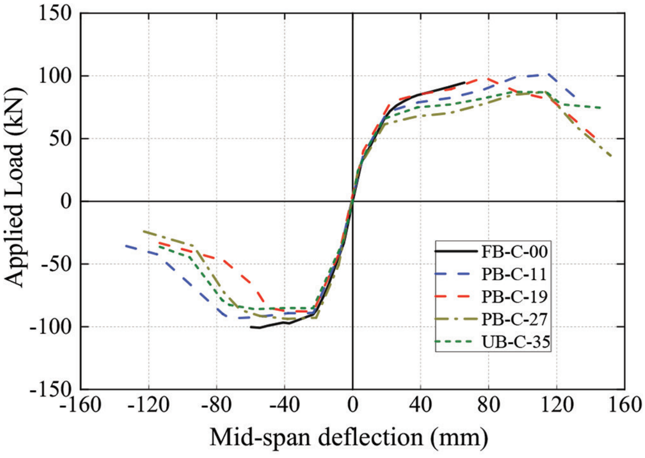

(a) CFRP prestressed concrete beams

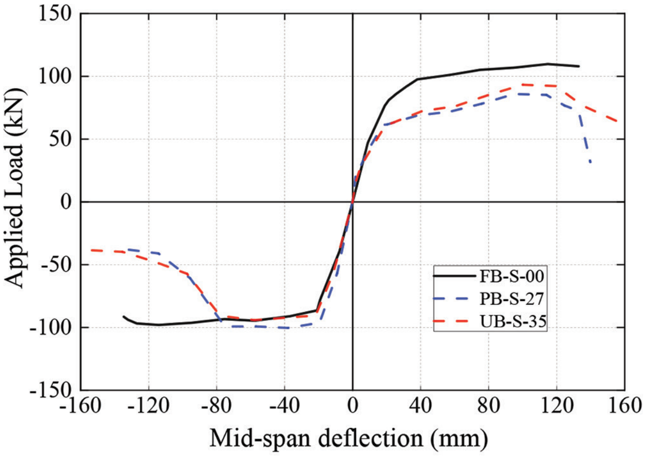

(b) steel prestressed concrete beams

Fig. 9—Skeleton curve. (Note: 1 kN = 0.2248 kip; 1 mm = 0.039 in.)

from 1100 to 2700 mm (43.3 to 106.3 in.), the P_{max} under downward loading decreased by 14.3%. This trend is expected as the unbonded portion allows for slippage, and the tendon strain at the peak load generally decreases as the unbonded length increases. Similar findings have also been reported in reinforced concrete beams strengthened with partially bonded near-surface-mounted FRP bars/strips (Sharaky et al. 2015; Choi et al. 2011b). When the unbonded length was beyond 2700 mm (106.3 in.), however, further increases in unbonded length had a negligible effect on P_{max}. It is important to note that the fully bonded CFRP prestressed beam (FB-C-00) exhibited a flexural capacity 8.0% lower than that of Specimen PB-C-11. This is because Specimen FB-C-00 experienced a premature failure due to rupture of CFRP before concrete crushing occurred. In contrast, an opposite trend was noticed in the prestressed beams with steel strands, where the maximum load capacity of the fully bonded prestressed beam (FB-S-00) was 29.0% higher than that of the partially bonded prestressed beam (PB-S-27). This is because both beams failed due to concrete crushing, and the stress in the fully bonded prestressed beam was higher than that in the partially bonded prestressed beam.

Displacement ductility

Ductility is a measure of the ability of a structural member to sustain large inelastic deformation without substantial decrease in load-carrying capacity. It serves as a warning sign before the occurrence of structural collapse. The ductility of a structural concrete beam can be expressed using the displacement ductility coefficient as follows

$$\mu = \frac{\Delta_u}{\Delta_y} \tag{2}$$

where Δ_y is the displacement corresponding to the yielding of the beam specimens; and Δ_u is the displacement at failure or the displacement corresponding to 80% maximum load in descending part of the skeleton curves, whichever is smaller (Park 1989). The measured Δ_u for each beam is provided in Table 4. When subjected to downward loading, the beams with the partially bonded CFRP tendon exhibited significantly higher deformability compared to the fully bonded CFRP prestressed concrete beam. This is due to the fact that the fully bonded beam exhibited a premature failure of CFRP rupture. Because the strains in the partially bonded tendon are relieved from critical sections and averaged out along the unbonded length, there was a trend that the deformability slightly increased as the unbonded length of the CFRP tendon increased.

The measured ductility coefficients of each beam are provided in Table 4, where only the ductility under downward loading was considered. The displacement ductility coefficients of partially bonded CFRP prestressed concrete specimens were in the range of 5.38 to 5.70, indicating that the specimens behaved in a relatively ductile manner. As observed in Table 4, the beams prestressed with steel strands displayed a more ductile behavior than those prestressed with CFRP strands. This can be attributed to the fact that CFRP possesses a linear elastic stress-strain relation and is inherently brittle in nature.

The bond condition had a significant effect on the displacement ductility of CFRP prestressed concrete beams under downward loading, as evident in Table 4. The displacement ductility of the partially bonded prestressed beams (PB-C-11, PB-C-19, and PB-C-27) was significantly higher than that of the fully bonded prestressed beam (μ = 2.83) and slightly lower than that of the fully unbonded prestressed beam (μ = 6.10). This is expected because the fully bonded prestressed beam failed due to rupture of the CFRP tendon, whereas the partially bonded and fully unbonded prestressed beams failed due to concrete crushing. Among the partially bonded prestressed beams tested, varying the unbonded length from 1100 to 2700 mm (43.3 to 106.3 in.) had an insignificant effect on the ductility, although the displacement ductility appeared to increase slightly increased with increasing the unbonded length.

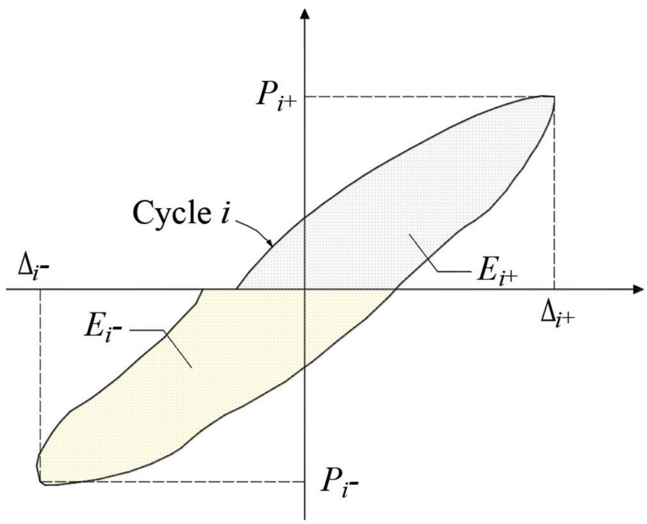

Fig. 10—Definition of energy dissipation.

Energy dissipation capacity

The energy dissipation capacity of a structural member is a valuable indicator for evaluating the seismic performance of the member. To quantify the energy dissipated during a single load cycle, the Trapezoid Rule was employed to calculate the area enclosed by the applied load versus midspan deflection curve. In Fig. 10, the shaded area represents the energy dissipation corresponding to the *i*-th loading cycle during downward or upward loading. It should be noted that the energy calculation for each step is the average of every three load cycles. The accumulated dissipated energy is obtained by summing up the shaded areas over the entire loading process.

Figure 11 shows the cumulative energy dissipated in each cycle for the tested beams. Initially, the accumulated energy dissipation remained relatively small until the midspan displacement reached Δ_y. As the applied displacement increased, the cumulative energy dissipation also increased. Up to a midspan displacement of $2\Delta_y$, the energy dissipated during upward loading was nearly equivalent to that during downward loading. Nevertheless, when the midspan displacement exceeded $3\Delta_y$, less energy was dissipated during upward loading compared to downward loading. This discrepancy can be attributed to the placement of the prestressing tendon at the bottom of the beam, resulting in significant overall strength degradation in the hysteresis loops during upward loading. Specimen FB-C-00, which experienced premature CFRP rupture, exhibited the lowest energy dissipation upon failure, accounting for approximately 25% of the energy dissipated in the partially bonded specimens. As depicted in Fig. 11(a) and (b), increasing the unbonded length of the prestressing tendons slightly reduced the cumulative energy dissipation. This can be attributed to the fact that prestressed beams with longer unbonded lengths exhibited lower load-carrying capacities. Figure 12 compares the cumulative energy dissipation in Specimen PB-C-27 (partially bonded CFRP tendon) with that in Specimen PB-S-27 (partially bonded steel tendon). Under identical loading cycles with the same downward displacements, the beam with the partially bonded CFRP tendon demonstrated a similar energy dissipation capacity to the beam with the partially bonded steel tendon, indicating that the fully bonded CFRP tendon beam exhibits a favorable energy dissipation capacity.

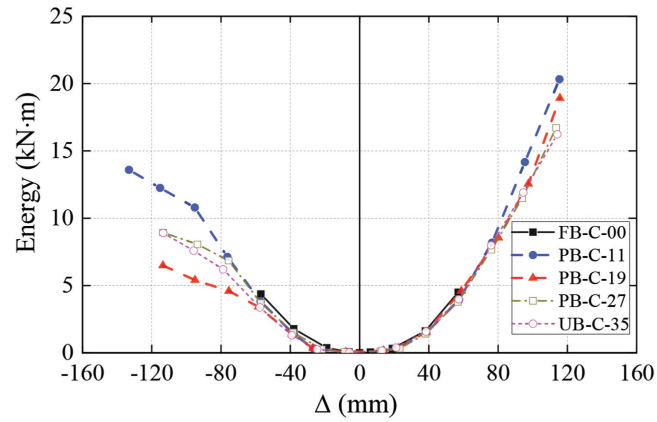

(a) CFRP prestressed concrete beams

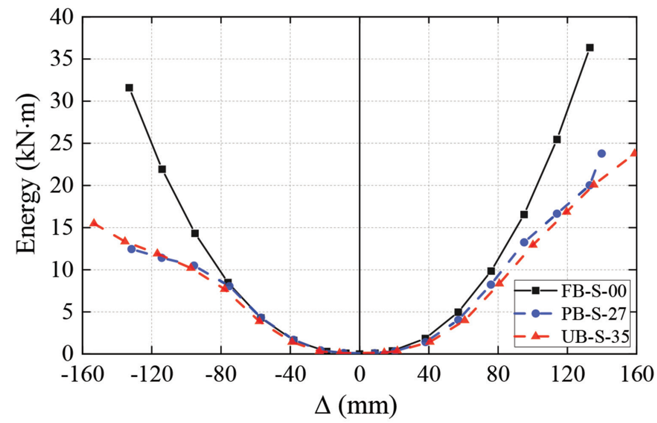

(b) Steel prestressed concrete beams

Fig. 11—Cumulative energy dissipation. (Note: 1 kN·m = 8.86 kip·in.; 1 mm = 0.0394 in.)

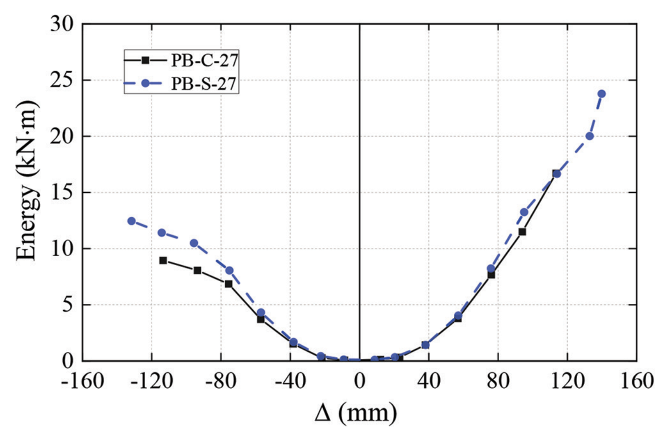

Fig. 12—Comparison of cumulative energy dissipation. (Note: 1 kN·m = 8.86 kip·in.; 1 mm = 0.039 in.)

DESIGN APPROACH FOR FLEXURAL CAPACITY

Currently, there is a lack of design guidelines for prestressed concrete beams with partially bonded CFRP tendons. In this study, the flexural design method previously

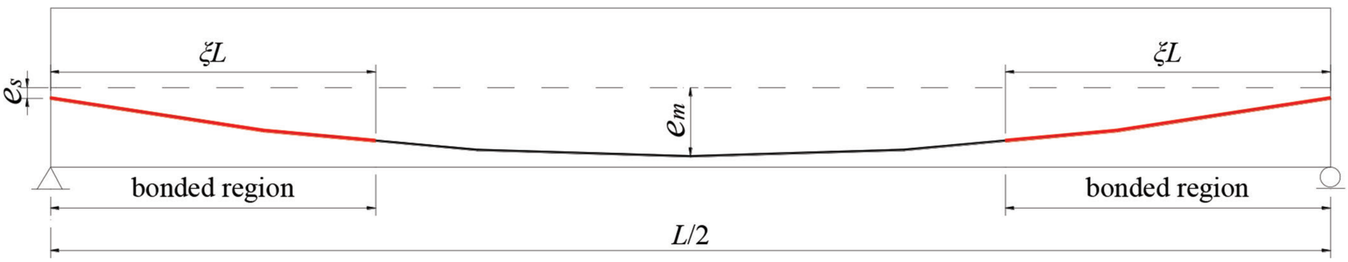

Fig. 13—Schematic diagram of partially bonded prestressed concrete beam.

developed by the authors (Peng and Xue 2019b) for fully unbonded post-tensioned concrete members was modified for predicting the flexural capacity of the partially bonded beams. This modified design method was used to predict the flexural capacity of the partially bonded beams. For partially prestressed beams with partially bonded CFRP tendons and nonprestressed steel bars, the flexural capacity can be determined by

$$M_u = A_s'f_y'\left(\frac{\beta_1 c}{2} - d_s'\right) + A_s f_y\left(d - \frac{\beta_1 c}{2}\right) + A_p f_p\left(d_p - \frac{\beta_1 c}{2}\right) \tag{3}$$

where A_s' is the area of steel bars in compression; b is the width of member; f_c' is the cylinder compressive strength of concrete; f_y' is the yield strength of steel bar in compression; f_p is the ultimate tensile stress in partially bonded or fully unbonded tendon; d_s' is the distance from the extreme compression fiber to the centroid of compression reinforcing bars; c is the distance from extreme compression fiber to the neutral axis at ultimate limit state; and β_1 is the ratio of depth of equivalent rectangular stress block to depth of neutral axis.

Because the ultimate stress in partially bonded tendons is member-dependent rather than section-dependent, an accurate prediction for the ultimate stress of the tendons is more difficult than that of bonded ones. The authors (Peng and Xue 2019b) have proposed an ultimate tensile stress equation for the unbonded tendon. For simplification, this equation was modified for the partially bonded tendon by introducing a relative bond length coefficient ξ (Fig. 13)

$$f_p = f_{pe} + \frac{E_p \varepsilon_{cu} e_m}{c}\frac{\chi}{(1-\xi)}\left(\frac{1}{f} + \frac{d_p}{L} + \frac{0.1Z}{L}\right)\left(1 + \frac{e_s}{e_m}\zeta\right) \tag{4}$$

where f_p is the ultimate tensile stress in the partially bonded tendon; f_{pe} is the effective prestressed stress; E_p is the elastic modulus of the tendon; e_m is the tendon eccentricity at beam midspan; e_s is the eccentricity at the support; L is the span length; Z is the shear span; χ is the normalized tendon elongation parameter, $\chi = 1 + 0.15(e_s/e_m - 1)^2 \leq 1.6$; ε_{cu} is the ultimate compressive strain of concrete; and $f = 10$ for a single concentrated load, 3 for two-third-point loads, and 6 for a uniform load application, respectively.

It should be mentioned that if the CFRP stress obtained from Eq. (4) is equal to or larger than the ultimate tensile strength f_{pu}, the expected failure mode is rupture of CFRP. Otherwise, concrete crushing will govern the failure. To compute f_p from Eq. (4), the value of depth of the neutral axis at ultimate limit state c should be computed. By considering the equilibrium of internal forces, the depth of neutral axis c can be solved by

$$A_s'f_y' + 0.85\beta_1 f_c'bc = A_s f_y + A_p f_p \tag{5}$$

Simultaneously solving Eq. (4) and (5) results in a quadratic equation in c with the following root

$$c = \frac{-B_1 + \sqrt{B_1^2 - 4A_1C_1}}{2A_1} \tag{6}$$

where $A_1 = 0.85\beta_1 f_c'b$; $B_1 = A_s'f_y' - A_s f_y - A_p f_{pe}$; and $C_1 = -A_p E_p \varepsilon_{cu} e_m \frac{\chi}{1-\xi}\left(\frac{1}{f} + \frac{d_p}{L} + \frac{0.1Z}{L}\right)\left(1 + \frac{e_s}{2e_m}\right)$

For partially bonded or fully unbonded prestressed concrete beams, Table 4 compares the predictions according to the presented design approach against the experimental maximum loads. In general, the predictions are in good agreement with the experimental results. The experimental load-carrying capacity is on average 1.00 of the predicted value, with a standard deviation of 6.6%.

SUMMARY AND CONCLUSIONS

In this study, eight post-tensioned concrete beams were tested to investigate the cyclic behavior of prestressed concrete beams with partially bonded carbon fiber-reinforced polymer (CFRP) tendons. Furthermore, a modified design approach for determining the flexural capacity of the beams was proposed. Based on the analysis of the experimental results, the following conclusions can be drawn:

1. Increasing the unbonded length of the CFRP tendons shifted the failure mode from CFRP tendon rupture to concrete crushing. The post-tensioned concrete beam with fully bonded CFRP tendons failed due to tendon rupture, while the post-tensioned beams with partially bonded or fully unbonded tendons failed due to concrete crushing.

2. There was a trend that the maximum loads decreased with increasing unbonded length of CFRP tendons.

3. The displacement ductility of partially bonded prestressed beams ranged from 5.38 to 5.70, which was significantly higher than that of the fully bonded prestressed beam (μ = 2.83) and slightly lower than that of the fully unbonded prestressed beam (μ = 6.10).

4. The partially bonded CFRP prestressed concrete beams exhibited acceptable energy dissipation capacity, and

increasing unbonded length of prestressing tendons would slightly decrease the accumulated energy dissipation.

5. The experimental flexural capacities were in close agreement with the values estimated using the proposed design approach for partially bonded prestressed concrete beams. The experimental flexural capacity was on average 1.00 of the predicted value, with a standard deviation of 6.6%.

AUTHOR BIOS

Fei Peng *is an Associate Professor in the College of Civil Engineering at Hunan University, Changsha, China, where he received his BS in 2013. He received his PhD from Tongji University, Shanghai, China, in 2019. His research interests include reinforced concrete structures with fiber-reinforced polymers and ultra-high-performance concrete structures.*

Weichen Xue *is the corresponding author and a Professor in the Department of Structural Engineering at Tongji University. He received his BS from Harbin Engineering University, Harbin, Heilongjiang, China, in 1990; his MS from Harbin Institute of Technology, Harbin, Heilongjiang, China, in 1992; and his PhD from Southeast University, Nanjing, Jiangsu, China, in 1995. His research interests include precast, prestressed concrete structures, and fiber-reinforced polymer composites.*

Shulu Zhang *is a Master's Student in the Department of Structural Engineering at Tongji University. He received his BS from East China Jiaotong University, Nanchang, Jiangxi, China, in 2004. His research interests include reinforced concrete structures.*

ACKNOWLEDGMENTS

The authors gratefully acknowledge the financial support of the Fund of the National Natural Science Foundation of China (No. 52130806 and No. 52008165).

REFERENCES

ACI Committee 440, 2004, "Prestressing Concrete Structures with FRP Tendons (ACI 440.4R-04)," American Concrete Institute, Farmington Hills, MI, 35 pp.

ASTM D7205-21, 2021, "Standard Test Method for Tensile Properties of Fiber Reinforced Polymer Matrix Composite Bars," ASTM International, West Conshohocken, PA, 13 pp.

Au, F. T. K., and Du, J. S., 2008, "Deformability of Concrete Beams with Unbonded FRP Tendons," *Engineering Structures*, V. 30, No. 12, pp. 3764-3770. doi: 10.1016/j.engstruct.2008.07.003

Chen, C.; Chen, J.; Zhou, Y.; Sui, L.; and Hu, B., 2021, "Design of Ductile H-Anchorage for Strengthening Reinforced Concrete Beams with Prestressed FRP," *Construction and Building Materials*, V. 307, Nov., p. 124883. doi: 10.1016/j.conbuildmat.2021.124883

Choi, H. T.; West, J. S.; and Soudki, K. A., 2011a, "Effect of Partial Unbonding on Prestressed Near-Surface-Mounted CFRP-Strengthened Concrete T-Beams," *Journal of Composites for Construction*, ASCE, V. 15, No. 1, Feb., pp. 93-102. doi: 10.1061/(ASCE)CC.1943-5614.0000149

Choi, H. T.; West, J. S.; and Soudki, K. A., 2011b, "Partially Bonded Near-Surface-Mounted CFRP Bars for Strengthened Concrete T-Beams," *Construction and Building Materials*, V. 25, No. 5, May, pp. 2441-2449. doi: 10.1016/j.conbuildmat.2010.11.056

Dorian, P. T., 2002, "Deformability and Ductility of Partially-Prestressed Concrete Beams Containing CFRP/Stainless Steel Reinforcements," master's dissertation, Queen's University, Kingston, ON, Canada, 255 pp.

Fischer, G., and Li, V. C., 2003, "Deformation Behavior of Fiber-Reinforced Polymer Reinforced Engineered Cementitious Composite (ECC) Flexural Members under Reversed Cyclic Loading Conditions," *ACI Structural Journal*, V. 100, No. 1, Jan.-Feb., pp. 25-35.

GB/T 50081, 2019, "Standard for Test Methods of Concrete Physical and Mechanical Properties (GB/T 50081-2019)," China Architecture & Building Press, Beijing, China, 103 pp.

GB/T 50152, 2012, "Standard for Test Method of Concrete Structures (GB/T 50152-2012)," China Architecture & Building Press, Beijing, China, 119 pp.

Grace, N. F., and Abdel-Sayed, G., 1998, "Ductility of Prestressed Concrete Bridges Using CFRP Strands," *Concrete International*, V. 20, No. 6, June, pp. 25-30.

Grace, N. F.; Ushijima, K.; Matsagar, V.; and Wu, C., 2013, "Performance of AASHTO-Type Bridge Model Prestressed with Carbon Fiber-Reinforced Polymer Reinforcement," *ACI Structural Journal*, V. 110, No. 3, May-June, pp. 491-501.

Heo, S.; Shin, S.; and Lee, C., 2013, "Flexural Behavior of Concrete Beams Internally Prestressed with Unbonded Carbon-Fiber-Reinforced Polymer Tendons," *Journal of Composites for Construction*, ASCE, V. 17, No. 2, Apr., pp. 167-175. doi: 10.1061/(ASCE)CC.1943-5614.0000306

Jeong, Y.; Kim, W. S.; Gribniak, V.; and Hui, D., 2019, "Fatigue Behavior of Concrete Beams Prestressed with Partially Bonded CFRP Bars Subjected to Cyclic Loads," *Materials (Basel)*, V. 12, No. 20, Oct., p. 3352. doi: 10.3390/ma12203352

Lee, C.; Shin, S.; and Lee, H., 2017, "Balanced Ratio of Concrete Beams Internally Prestressed with Unbonded CFRP Tendons," *International Journal of Concrete Structures and Materials*, V. 11, No. 1, pp. 1-16. doi: 10.1007/s40069-016-0171-6

Lees, J. M., and Burgoyne, C. J., 1999, "Experimental Study of Influence of Bond on Flexural Behavior of Concrete Beams Pretensioned with Aramid Fiber Reinforced Plastics," *ACI Structural Journal*, V. 96, No. 3, May-June, pp. 377-385.

Park, R., 1989, "Evaluation of Ductility of Structures and Structural Assemblages from Laboratory Testing," *Bulletin of the New Zealand National Society for Earthquake Engineering*, V. 22, No. 3, pp. 155-166. doi: 10.5459/bnzsee.22.3.155-166

Peng, F., and Xue, W., 2018a, "Design Approach for Flexural Capacity of Concrete T-Beams with Bonded Prestressed and Nonprestressed FRP Reinforcements," *Composite Structures*, V. 204, pp. 333-341. doi: 10.1016/j.compstruct.2018.07.091

Peng, F., and Xue, W., 2018b, "Analytical Approach for Flexural Capacity of FRP Prestressed Concrete T-Beams with Non-Prestressed Steel Bars," *Journal of Composites for Construction*, ASCE, V. 22, No. 6, p. 04018063. doi: 10.1061/(ASCE)CC.1943-5614.0000903

Peng, F., and Xue, W., 2019a, "Reliability-Based Design Provisions for Flexural Strength of Fiber-Reinforced Polymer Prestressed Concrete Bridge Girders," *ACI Structural Journal*, V. 116, No. 1, Jan., pp. 251-260. doi: 10.14359/51710876

Peng, F., and Xue, W., 2019b, "Calculating Method for Ultimate Tendon Stress in Internally Unbonded Prestressed Concrete Members," *ACI Structural Journal*, V. 116, No. 5, Sept., pp. 225-234. doi: 10.14359/51716764

Peng, F.; Xue, W.; and Yu, T., 2023, "Cyclic Behavior of Polypropylene Fiber Reinforced Concrete Beams with Prestressed CFRP Tendons and Nonprestressed Steel Bars," *Engineering Structures*, V. 275, Jan., p. 115201. doi: 10.1016/j.engstruct.2022.115201

Poudel, P.; Belarbi, A.; Gencturk, B.; and Dawood, M., 2022, "Flexural Behavior of Full-Scale, Carbon-Fiber-Reinforced Polymer Prestressed Concrete Beams," *PCI Journal*, V. 67, No. 5, Sept.-Oct., pp. 22-39. doi: 10.15554/pcij67.5-01

Rizkalla, N. S., 2000, "Partial Bonding and Partial Prestressing Using Stainless Steel Reinforcement for Members Prestressed with FRP," master's dissertation, Queen's University, Kingston, ON, Canada, 212 pp.

Safan, M. A., 2013, "Flexural Behavior and Design of Steel-GFRP Reinforced Concrete Beams," *ACI Materials Journal*, V. 110, No. 6, Nov.-Dec., pp. 677-685.

Sharaky, I. A.; Torres, L.; and Sallam, H. E. M., 2015, "Experimental and Analytical Investigation into the Flexural Performance of RC Beams with Partially and Fully Bonded NSM FRP Bars/Strips," *Composite Structures*, V. 122, pp. 113-126. doi: 10.1016/j.compstruct.2014.11.057

Sun, Y.; Wu, T.; Liu, X.; and Zhang, B., 2022, "Failure Mode and Flexural Capacity of Concrete Beams Prestressed with Unbonded FRP Tendons," *Composite Structures*, V. 283, p. 114956. doi: 10.1016/j.compstruct.2021.114956

Xue, W.; Cheng, B.; Zheng, R.; Li, L.; and Li, J., 2011, "Seismic Performance of Nonprestressed and Prestressed HPC Frames under Low Reversed Cyclic Loading," *Journal of Structural Engineering*, ASCE, V. 137, No. 11, pp. 1254-1262. doi: 10.1061/(ASCE)ST.1943-541X.0000367